JOURNAL OF PROPULSION AND POWER
Vol. 16, No. 5, September–October 2000

# Analysis of Transient Thermal Choking Processes in a Model Scramjet Engine

S. O'Byrne,* M. Doolan,† S. R. Olsen,† and A. F. P. Houwing‡
*Australian National University, Canberra, Australian Capital Territory 0200, Australia*

**Shadowgraph flow visualization and floor static pressure measurements have been used to examine the transient behavior of a thermally choked combusting flow. Experiments were performed to examine the effect of varying inlet Mach number and fuel–air equivalence ratio on the nature and extent of the interaction. In all cases a sudden increase in static pressure was measured, followed by a highly turbulent region of sonic flow that was seen to propagate upstream along the duct. The nature of the dominant processes causing this pressure discontinuity are still not certain. Some mechanisms that may contribute to this phenomenon are presented. These include separation of the boundary layer in the duct, formation of a detonation, and formation of a near-normal shock wave by the region of thermally choked flow.**

## Introduction

IT is essential to the design of supersonic-combustion ramjet (scramjet) engines that the fuel–air mixture remains supersonic throughout the combustor. If the heat released by the combustion process becomes greater than a critical value, the Mach number in the engine falls to unity, and the flow becomes thermally choked.[1] This choked flow may in turn cause a normal shock to form at the engine inlet. This process, known as unstart, creates large amounts of drag and radically reduces the performance of the engine at high flight Mach numbers.

The experiments described herein were performed to examine the nature of the processes that lead to unstart in a thermally choked combusting environment at different combustor entrance Mach numbers and fuel–air equivalence ratios.

The phenomena described were first noted in studies of supersonic combustion, whose results have been presented elsewhere.[2] It was noted in those tests that when a constant-area combustor was employed, a rise in static pressure occurred that was much greater than that due to supersonic combustion. It is the aim of this paper to outline the nature of the observed phenomena accompanying this pressure rise and to present some possible mechanisms for its generation.

## Experimental Arrangement

### Generation of Inlet Conditions

The high flow velocities and enthalpies required to simulate the conditions necessary for scramjet flight were generated using the T3 free-piston shock tunnel facility at the Australian National University,[3] operating in reflected shock mode. The experiments were performed at two flow conditions, with Mach numbers of 2.5 and 3.8 at the combustor entrance. These conditions were designed to simulate the flow in a scramjet engine operating at flight Mach numbers of approximately 6 and 9. The combustor-entrance conditions are outlined in Table 1.

The Mach 3.8 condition was produced using a contoured nozzle with an exit diameter of 90 mm and an exit-to-throat area ratio of 12.2. If the Mach 2.5 condition flow were generated using a nozzle, the required area ratio would be 2.6. To produce a flow that would occupy the whole of the model scramjet duct, the throat of the nozzle would have nearly the same diameter as the shock tube itself. Thus, the Mach 2.5 combustor inlet flow was generated using a variable-angle supersonic diffuser downstream of a Mach 5.5 conical nozzle. This arrangement is shown in Fig. 1.

The angled top and bottom plates of the diffuser act to compress the flow from the nozzle and reduce its Mach number, by the formation of a pair of oblique reflecting shock waves. The Mach number of the flow at the exit of the diffuser could, thus, be controlled by varying the angle of the diffuser plates. The placement of the diffuser 21 mm upstream of the scramjet model inlet was determined by the need for the shock waves at the diffuser exit to pass outside the combustor duct.

The Mach number at the combustor entrance was measured by obtaining shadowgraph images of Mach waves formed in the empty scramjet combustor duct. The plates were oriented at an angle of 15.5 deg to the horizontal to obtain an entrance Mach number of $2.5 \pm 0.1$.

Pitot and static pressure measurements at the duct entrance were used, along with knowledge of the Mach number, to determine the conditions at the duct entrance. The shock tube fill conditions were varied until the values presented in Table 1 were achieved. These measurements also showed that the total pressure varied by less than 5% during the test time and less than 10% across the entrance to the scramjet duct, ensuring that the flow entering the duct was uniform throughout the test time.

### Scramjet Model

The model scramjet engine was a rectangular duct with central strut injection, as shown in Fig. 2. This model can be used as a constant cross-sectional area duct, as shown in Fig. 2a, or a varying cross-sectional area duct, as shown in Fig. 2b. The constant-area duct was used for tests at both conditions, whereas the varying cross-sectional area duct was used for the Mach 2.5 condition. The same model has been used in previously published experimental studies.[2,4,5] The constant-area duct had a $25 \times 50$ mm cross section and was about 400 mm in length, whereas the varying cross-sectional duct had a 3.5-deg diverging section that commenced 187 mm from the inlet. The injector was 4.8 mm thick and had a plane base, from which fuel was injected through a rectangular slot. Injection of hydrogen fuel into the flow was achieved using a Ludweig tube and fast-acting valve arrangement.[6] The valve was triggered by the recoil of the tunnel and was set so that injection occurred several milliseconds before the onset of the airflow from the shock tunnel. The fuel–air equivalence ratio was varied by increasing or decreasing the pressure in the injector plenum chamber, which in turn varied the mass flow rate of fuel through the injector.

Optical access to the combustor was provided by a pair of glass windows in the side walls of the duct. This permitted visualization of a length of duct extending 180 mm downstream of the injector exit.

Received 20 January 1998; revision received 20 August 1999; accepted for publication 25 August 1999. 

*Postgraduate Student, Department of Physics, Faculty of Science.
†Undergraduate Student, Department of Physics, Faculty of Science.
‡Senior Lecturer, Department of Physics, Faculty of Science. Member AIAA.

**Table 1 Flow properties in shock tube and combustor inlet for scramjet tests**

| | Mach 3.8 condition | | Mach 2.5 condition | |
|---|---|---|---|---|
| Property | Reservoir[a] | Entrance[b] | Reservoir[a] | Entrance[b] |
| $P$, kPa | 19,000 | 110 | 9,500 | 100 |
| $T$, K | 3,200 | 1,100 | 2,500 | 1,200 |
| $V$, m/s | —— | 2,390 | —— | 1,710 |
| $H_0$, MJ/kg | 3.8 | —— | 2.8 | —— |

[a]Shock tunnel reservoir conditions. [b]Conditions at combustor entrance.

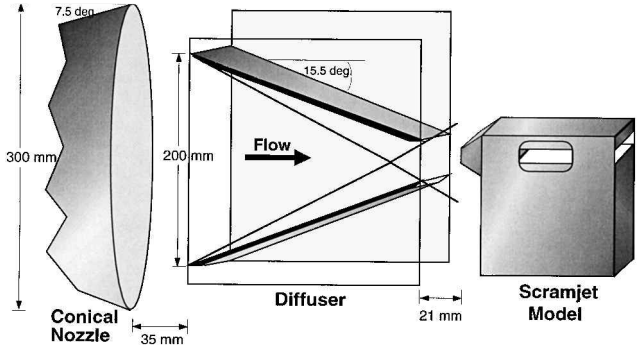


**Fig. 1 Schematic of the conical nozzle/diffuser arrangement used to generate the inlet flow at the Mach 2.5 condition; flow proceeds from left to right.**

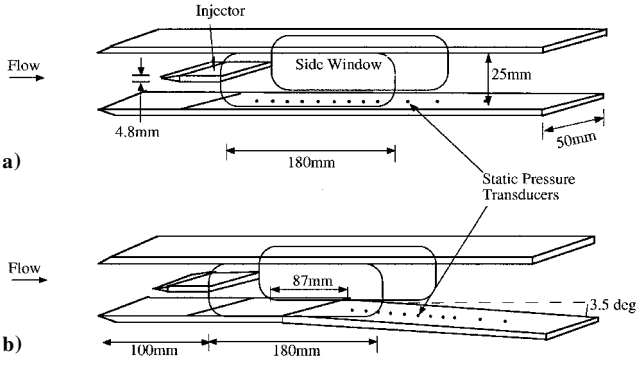


**Fig. 2 Schematic of the scramjet model: a) constant-area duct used for tests at both conditions and b) duct with 3.5-deg diverging section used for Mach 2.5 condition test to prevent choking.**

Pressure transducers (PCB-type 113M65) were distributed longitudinally along the center of the duct floor from a distance of 50 mm downstream of the injector exit to the end of the duct.

### Shadowgraph Visualization System

A single-pass shadowgraph system was employed for visualization of the flowfield, as shown in Fig. 3. Illumination for the images was provided by a single 500-ns pulse from a flashlamp-pumped dye laser. The pulse length was of sufficiently short duration to allow an instantaneous image of the flow to be obtained. The beam was expanded and collimated, passed through the test section, and imaged on a Kodak TMax 400 film plate. The sensitivity of the resulting image to variations in density could be increased, at the cost of definition, by focusing the image at the film plate away from the center of the test section. The imaging position could be varied by varying the axial position of the lens in front of the film plate.

## Results

To uncouple the effects of mixing from those of combustion, all tests were performed twice: the first time with injection of hydrogen fuel into a nitrogen freestream (to examine flow without combustion) and then with injection into an air freestream. Static-pressure distributions and shadowgraph images were obtained for each of these tests.

To determine when the scramjet duct flow starts, static pressure measurements were made inside the duct for the case of no combustion (injection into nitrogen), and the measured values were normalized with the nozzle reservoir pressure trace in a manner that took into account the nozzle transit time. As explained by Casey,[7] a constant value of the normalized static pressure indicates that the Mach number (and, hence, other dimensionless quantities of importance) is constant, and therefore, the duct flow has established. These considerations indicate that the scramjet duct flow starts at 1.5 ms after shock reflection for the Mach 3.8 condition and at 2 ms after shock reflection for the Mach 2.5 condition.

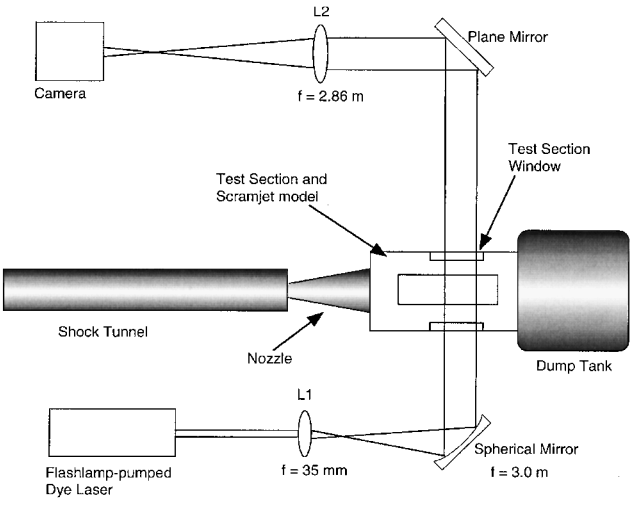


**Fig. 3 Schematic of the single-pass shadowgraph system.**

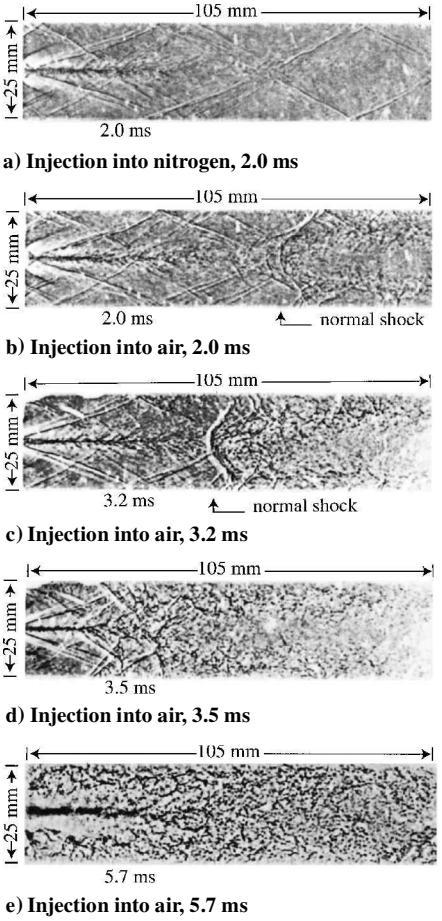


**Fig. 4 Shadowgraph images, equivalence ratio $\phi = 0.4$, of flow at Mach 2.5 combustor-inlet condition.**

### Mach 2.5 Condition

Shadowgraph images for the Mach 2.5 inlet flow are presented in Fig. 4. In each of the images, injection occurs at the extreme left of

the image and flow is from left to right. The time delay beside each picture indicates the time after measured shock reflection when each image was obtained. Figure 4a is a typical image for injection into a nitrogen freestream. The main features apparent in this image are the wake recompression shock waves and the shock waves arising from the leading edge of the injector, which can be seen to propagate along the duct. The existence of these shock waves indicates that flow is supersonic throughout the visible region of the duct for the case of injection into nitrogen. The lighter regions in the upstream portion of the image indicate the presence of an expansion wave caused by expansion of the flow around the base of the injector. The fuel jet is evident as a dark region that extends a distance of approximately 50 mm downstream of the injector exit, after which it is obstructed by the wake of the injector. Less sensitive shadowgraph images show that the jet may be seen throughout the visible part of the duct. Thus, mixing between the fuel and nitrogen streams is significantly poorer than Fig. 4a might initially suggest.

Figures 4b–4e are shadowgraph images obtained for injection into air at an equivalence ratio $\phi$ of 0.4, at different times. The times indicated on the image are determined relative to the time at which the shock reflects from the shock tunnel's nozzle reservoir. Figure 4b is similar in the upstream-half of the visible duct to the image for injection into nitrogen, but there is an obvious difference between the two images in the downstream-half of the duct. At the point where the wake recompression shock waves intersect, a shock wave occurs that is oblique in the top and bottom parts of the duct and nearly normal to the flow in the jet/wake region. Flow downstream of this shock wave in the central part of the duct appears to be much more turbulent than that in the upstream part of the image. The normal shock in Fig. 4b actually looks like two normal shocks, one downstream of the other. However, as a result of careful examination of the image, we conclude that it appears that way because the shock is in fact curved and that the line-of-sight visualization method highlights the upstream and downstream portions of the shock.

The situation shown in Fig. 4b remains stable for less than a millisecond, after which the shock wave becomes stronger in appearance and begins to propagate upstream along the duct toward the injector exit. The propagation of the disturbance is shown in Figs. 4c and 4d. As it proceeds along the duct, the shock generates a region of highly turbulent combusting flow downstream of it. At a delay time of 5.7 ms (Fig. 4e), the flow downstream of the injector exit appears entirely turbulent, with no evidence of the oblique shock waves evident in the previous images. Note that the region of turbulence does not propagate any farther upstream than the exit of the injector. The upstream portion of the region of turbulence is directly correlated with the large pressure rise that propogates upstream and then becomes stationary at the injector exit. Evidence that this region does not propogate upstream of the injector exit is provided through pressure measurements by a transducer located upstream of the injector base.

Tests performed at higher fuel–air equivalence ratios than those shown in Fig. 4 produced shadowgraphs similar to that in Fig. 4e immediately after the onset of the flow.

A sample pressure trace for a transducer in the $\phi = 0.4$ experiments is shown in Fig. 5. The pressure for injection into air is consistently higher than that for injection into nitrogen. The difference between the pressures is due to the heat release arising from combustion. There is clearly a two-stage pressure increase in Fig. 5. The first increase in static pressure for injection into air over injection into nitrogen is due to supersonic combustion. At about 3.5 ms, a second pressure increase is apparent that is much larger than the first. The timing of this second pressure rise corresponds, at each transducer, to the passing of the shock wave shown in Fig. 4 over the transducer. Pressure measurements in the region downstream of the visible portion of the duct in Fig. 4 show exactly the same two-stage pressure rise, with the second pressure rise occurring nearly simultaneously for all transducers downstream of the visible portion of the duct. For equivalence ratios greater than 0.4, the pressure traces show only a single pressure rise, of the same magnitude (relative to the pressure for injection into nitrogen) as the second pressure rise in Fig. 5.

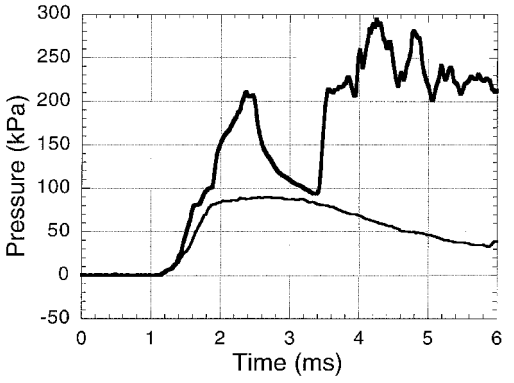


**Fig. 5 Floor static pressure trace for $\phi$ = 0.4 injection into air (upper trace) and nitrogen (lower trace) for a transducer located 54 mm downstream of the injector exit.**

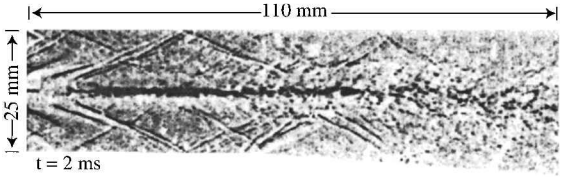


**Fig. 6 Shadowgraph of injection into air at $\phi$ = 1.7 with divergent duct geometry for a time of 2 ms after shock reflection.**

It is also apparent from Fig. 5 that the static pressure remains constant (when normalized to the pressure measured for injection into nitrogen) after the second pressure rise.

Subsequent experiments were performed using a duct whose floor diverged at an angle of 3.5 deg to the horizontal, as shown in Fig. 2b. Previous investigations[1,8] have shown that thermally induced choking at low combustor-entrance Mach numbers can be prevented using such a divergence in the combustor. Using this divergence angle prevented the second pressure rise that was in evidence for all of the straight duct tests. Tests of the diverging duct geometry were performed at the Mach 2.5 condition for equivalence ratios of up to 2.2, and the second pressure rise was successfully prevented in all tests.

Figure 6 shows a shadowgraph image of injection into air at $\phi = 1.7$ using the diverging combustor geometry shown in Fig. 2b for a time of 2 ms after shock reflection. The expansion wave caused by the divergence in the floor can be seen halfway along the shadowgraph image. The very turbulent flow apparent in Fig. 4 cannot be seen in this image and evidence of the existence of shock waves was noticed throughout the visible part of the duct, indicating that the combustion remained supersonic.

Static pressure, normalized to the pressure for injection into nitrogen, is given as a function of distance downstream of the injector in Fig. 7. Equivalence ratios of 0.4 and 1.7 using a constant-area duct and 1.7 using a divergent duct are included in the graph.

Combustion with the diverging duct geometry generates a pressure rise of approximately 200% throughout the test time. This is comparable with the pressure rise that occurs for supersonic combustion in the straight duct at $\phi = 0.4$, but is much less than the 350–400% rise for $\phi = 1.7$ with the straight duct. This result implies that supersonic combustion can be achieved with high equivalence ratios using a divergent duct geometry.

The divergent section of the duct used to obtain the results presented in Fig. 7 was located about 50 mm from the exit of the injector. It is apparent from Fig. 7 that the pressure increase due to combustion occurs in the diverging section of the duct.

### Mach 3.8 Condition

Experiments were also performed for the Mach 3.8 combustor-entrance condition, in the same manner as those described in the preceding section. Flows with equivalence ratios of 0.25, 0.5, and

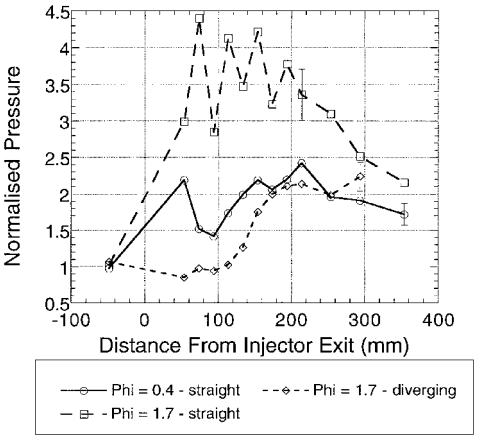


**Fig. 7 Comparison of static pressure measurements (normalized to pressure for injection into nitrogen) plotted as a function of distance along the duct at $t$ = 2.0 ms after shock reflection.**

1.0 were examined. The shock tube reservoir and scramjet duct entrance flow properties for the Mach 3.8 condition are shown in Table 1.

The essential nature of the observed choking phenomena was the same for these experiments as for the Mach 2.5 condition experiments. In both series of experiments there was a two-stage increase in static pressure. The main difference between results obtained at the different inlet conditions was that the second pressure rise occurred much later in the flow time and was significantly larger (when normalized to the pressure measured for injection into nitrogen) in the Mach 3.8 case than for the tests performed at a Mach number of 2.5.

The larger pressure rise was measured at all equivalence ratios tested. The choking of the flow at the Mach 3.8 condition occurred between 5 and 8 ms after shock reflection, depending on the equivalence ratio of the test. Low equivalence ratio tests choked at a later time than tests at higher equivalence ratios.

The pressure discontinuity at the Mach 3.8 condition occurred during that part of the flow where the presence of driver gas had a significant effect upon the flow properties. Measurements of Mach angle throughout the flow time were made using the shadowgraph system and were used to determine the percentage of driver gas contamination throughout the flow time. The percentage of driver gas contamination was determined as follows. The Mach angle was used to determine the Mach number of the flow inside the duct at the exit of the supersonic nozzle. This Mach number depends on the ratio of specific heats through the theory for an isentropic expansion of a perfect gas through the shock tunnel nozzle. Because the ratio of specific heats for the test and driver gases are significantly different, the ratio of the specific heats of a mixture will depend on the percentage of driver gas contamination. Thus, the Mach number measurement enabled us to determine the ratio of specific heats, from which we could determine the amount of driver gas contamination. These measurements showed the arrival of driver gas to occur between 4 and 6 ms after shock reflection. At 8 ms after shock reflection, driver gas comprised 60 ± 20% by volume of the fluid in the duct. The choking phenomenon at the higher Mach number condition was, thus, complicated by the presence of driver gas in the duct.

Shadowgraph images of the flow during the choking process are shown in Fig. 8. Again, flow is from left to right and times indicate time after measured shock reflection when each image was obtained. Figure 8a is a typical shadowgraph image for injection into nitrogen. As for the Mach 2.5 inlet condition, the existence of shock waves throughout the duct indicates that the flow is supersonic. The shocks are shallower than those in Fig. 4 because of the higher freestream Mach number.

Figure 8b illustrates the flow as supersonic combustion occurs in the duct. There is apparent a region of turbulence in the injector wake flow that propagates downstream as a flame in the visible part

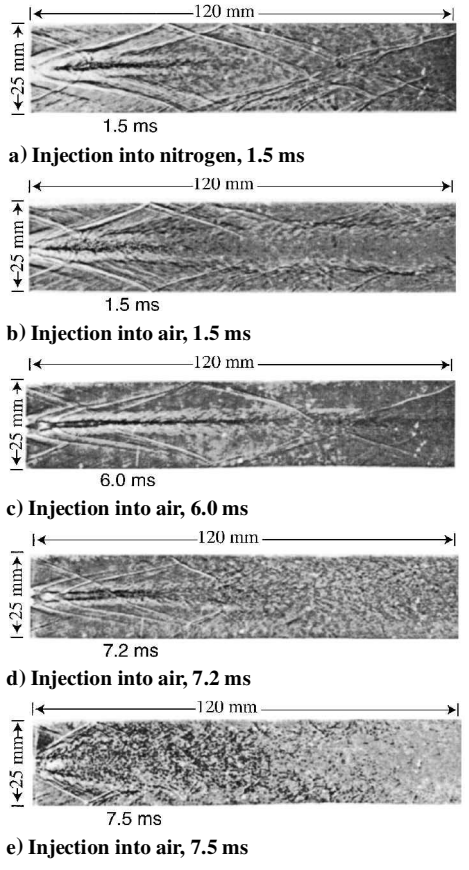


**Fig. 8 Shadowgraph images of flow at Mach 3.8 combustor-entrance condition at an equivalence ratio of 0.5.**

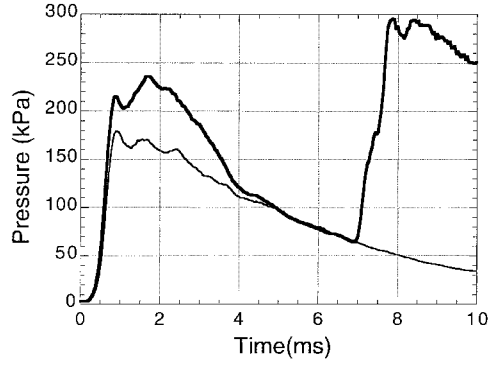


**Fig. 9 Floor static pressure trace for $\phi$ = 0.5 injection into air (upper trace) and injection into nitrogen (lower trace) for a transducer located 76 mm downstream of the injector exit.**

of the duct. The flow remains supersonic in the regions closest to the floor and ceiling of the duct, where shock waves can still be seen.

Figure 8c shows the flow for injection into air at 6 ms after shock reflection. The flow at this time looks very similar to that for injection into nitrogen. The turbulent flame that is apparent in the earlier image has vanished, indicating that combustion is not occurring in the visible part of the duct.

Approximately 7.2 ms after shock reflection, a second rise in static pressure is measured by the transducers and moves upstream along the duct, choking the flow behind it. Shadowgraph images of this pressure disturbance are shown in Figs. 8d and 8e. Essentially, the pressure discontinuity appears to be the same as that observed in the Mach 2.5 tests. It appears to be convex and driven upstream from within the wake region of the flow. The pressure rise does not propagate upstream of the injector exit.

Figure 9 shows a static pressure trace for a transducer in the visible portion of the duct. The pressure history for injection into air

provides good agreement with the shadowgraph images in Fig. 8. An initial pressure rise corresponding to supersonic combustion is followed by a period of flow in which no combustion is measured by the transducers in the visible part of the duct, presumably because of the reduction in static pressure and temperature in the freestream at the time. The increased angle of the shock waves indicates an increase in Mach number caused by driver gas contamination at this time. This continues until approximately 7 ms after shock reflection, when a second, much larger pressure rise occurs.

Pressure transducers downstream of the visible part of the duct show a pressure rise for the entire flow time, indicating that combustion occurs in the downstream part of the duct throughout the measurement time.

## Discussion of Results

The complexity of the flowfield and the competition between the effects of fluid dynamics, combustion, and driver gas contamination make it difficult to link the pressure history and visual information from the shadowgraph images with the dominant choking processes. This section presents some mechanisms that may cause the observed pressure discontinuity.

The observation that the pressure discontinuity only occurs for injection into air is an indication that it is caused by the combustion occurring downstream of it. The pressure rise occurs at both the Mach 2.5 and Mach 3.8 combustor-entrance conditions, and the shadowgraph images are similar in nature at both conditions, which indicates that driver gas contamination is not the primary cause of the pressure rise. Contamination does, however, have an effect on the propagation of the discontinuity because a higher ratio of specific heats will cause a faster shock propagation velocity.

Another important finding, based on the measured static pressure distributions, is that the flow downstream of the pressure discontinuity is choked. A one-dimensional finite difference calculation, based on the treatment in Ref. 9, was used to determine the Mach number as a function of distance along the duct floor at the time each of the shadowgraph images was obtained. The measured pressure distribution, combined with knowledge of all of the flow properties at the combustor entrance, allowed velocity, density, and Mach number distributions to be obtained. The Mach number distributions are the most significant to the present discussion, and so only these will be presented. The computed Mach number distributions should be viewed with caution because a one-dimensional calculation does not account for the presence of two-dimensional (oblique) shocks. However, the calculation does account for heat release and the dilution of the test gas caused by driver gas contamination.

Figures 10 and 11 are the results of the calculation of average Mach number along the duct for the Mach 2.5 and Mach 3.8 conditions, respectively. The upper line in Fig. 10 shows the Mach number distribution for 2 ms after shock reflection, whereas the lower line indicates the distribution after the shock has passed through most of the visible portion of the duct. This graph shows very clearly that the flow in the duct is sonic after being processed by the shock.

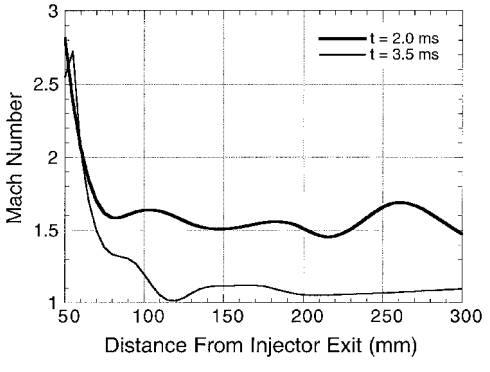


**Fig. 10 Mach number as a function of distance from the injector exit for the Mach 2.5 combustor-entrance condition.**

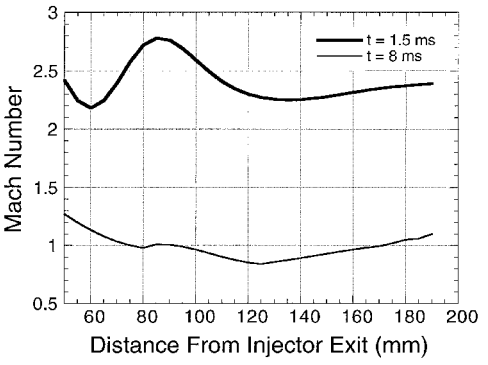


**Fig. 11 Mach number distribution for the Mach 3.8 combustor-entrance condition.**

Figure 11 shows that the Mach number also decreases to unity at the Mach 3.8 entrance condition after being processed by the shock. At that condition, the change is even more noticeable.

The observation that, at both conditions there is an abrupt change from supersonic to sonic flow is an indication that the shock wave is a manifestation of choked flow in the downstream part of the duct. Because the phenomenon only occurs for injection into air, the choking process must be caused by heat release. Two questions that remain, however, are what causes the shock to propagate upstream and whether the combustion of the flow processed by the shock wave has a significant effect on the shock wave propagation.

There are two possible processes leading to the formation of the shock wave apparent in Figs. 4 and 8. It may be caused by shock-induced separation of the boundary layer in the duct or by a sudden deceleration of the flow upstream of a region of intense heat release.

In an area of the flow where there exists a region of the boundary layer experiencing an adverse pressure gradient, the boundary layer can separate. This is usually caused by the sudden pressure discontinuity across a shock wave. Once the boundary layer separates, a series of oblique shock waves form that can choke the flow and propagate upstream along the duct. Reference 10 contains a summary of experimental results relating shock-induced separation at a particular Mach number to a minimum pressure ratio across the shock. The pressure rise across the shock waves for injection into nitrogen is insufficient to separate the boundary layer, but it is possible that heat release for the case of injection into air could provide larger local pressure gradients than those required (2.5 and 4.5 times for the Mach 2.5 and Mach 3.8 conditions, respectively). Certainly, the measured pressure difference between injection into air and nitrogen is greater than that required for shock-induced separation (4.5 and 8 times for the Mach 2.5 and Mach 3.8 conditions, respectively).

There is evidence (particularly apparent in Fig. 4d) that the boundary layer separates when the wave is propagating upstream, because of the size of the pressure gradient across it. Note, however, that the shape of the shock wave during its formation (Fig. 4b) is not consistent with formation by boundary-layer separation. If the shock were formed by separation of the boundary layer in the duct floor, there would form a system of oblique shock waves, terminated by a single normal shock wave downstream of them.[1,11] Figure 4b shows a single near-normal shock in the wake region of the flow, which is more oblique near the upper and lower duct walls.

Therefore, it appears that deceleration of the flow in the wake region due to large amounts of heat release is more likely to cause the shock wave than wall boundary-layer separation. If this is the case, then there still remains the question of whether or not the heat release is directly coupled to the upstream motion of the shock wave. The heat release may be merely acting as a physical flow restriction, in the same way as a blockage in the duct might cause the supersonic flow to become mechanically choked. The assumption that heat release acts in a manner that is analogous to a physical flow restriction has formed the basis of previous analytical[11] and experimental[12] studies of thermal choking in scramjet combustors. The shadowgraph images obtained in these experiments indicate,

however, that combustion downstream of the shock wave may have an effect on its propagation.

The shock is most normal in the wake region of the flow, and this part of the shock wave accelerates with respect to the outer parts of the shock wave, as shown in Fig. 4. This behavior indicates that heat release in the wake may be pushing the shock wave upstream. It has been mentioned in previous experiments[13] that there can exist regions in the mixing layer where very high local temperatures are generated by heat release. If the temperature gradient is large enough in such a region, the flow may become subsonic because of the increase in sound speed, even in the absence of a pressure gradient. Such a process may, according to Ref. 13, generate a region of highly unstable recirculating flow. It is certainly conceivable that the reflection of the wake recompression shock waves might generate such a region of high-temperature reacting flow that may in turn release sufficient heat to drive the shock wave upstream. If the heat release were sufficiently large, the shock may become a detonation wave.

In an attempt to determine whether the combustion had an effect on the propagation of the wave itself, the wave velocities were measured for both combustor-entrance Mach number conditions. The wave propagation speed was determined from the experimental results by examining the temporal variation of the measured pressure ratios. Figures 12 and 13 are plots of distance of the shock from the injector exit against the time after shock reflection for the Mach 2.5 and Mach 3.8 conditions, respectively. For each Mach number and equivalence ratio tested, the shock speed was measured several times and was found to be consistent. The measured velocity varied in each case by less than 10 m/s.

Unsteady one-dimensional supersonic flow theory can be used to relate the propagation speed of a normal shock to the pressure ratio across it and the ratio of specific heats. Such an analysis can predict the wave propagation speed if it were independent of heat-release effects. The predicted velocity for the Mach 2.5 condition is 1500 m/s and for the Mach 3.8 condition is 2550 m/s, relative to the freestream. This compares well to the 2500–2550 m/s measured at the Mach 3.8 condition, but is significantly lower than the measured velocity of 1800 m/s indicated in Fig. 12. This may indicate that the effect of heat release on propagation speed is significant at the lower Mach number condition, but is less important for the higher Mach number condition.

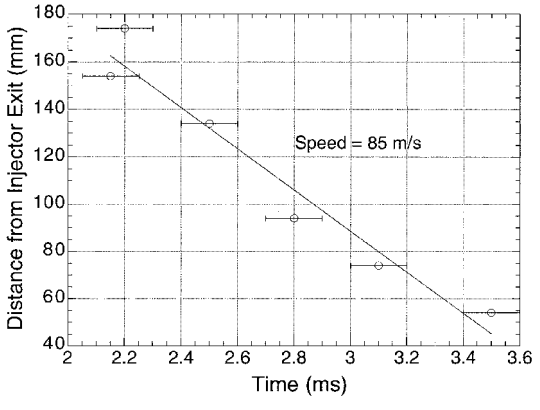


**Fig. 12 Shock speed for diffuser condition, $\phi = 0.4$.**

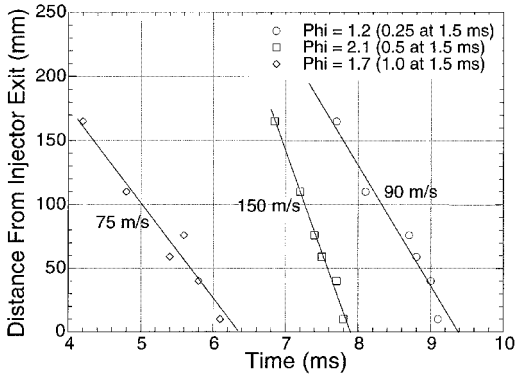


**Fig. 13 Shock propagation speed for Mach 3.8 combustor-inlet condition.**

Close examination of Fig. 13 shows that the wave velocity varies measurably, depending on the equivalence ratio. The values of $\phi$ shown in Fig. 13 are different to the values measured during the constant flow time (1.5 ms after shock reflection) because of the decrease in the mass flow rate of air and the increasing percentage of driver gas in the duct at the later delay times. The equivalence ratio at the constant flow time is shown in parentheses.

The variation of wave speed reflects the complexity of the interaction between effects of heat release and those of driver gas contamination. The presence of helium driver gas in the flow will cause the wave to speed up due to a higher ratio of specific heats and will also increase the effective equivalence ratio, but the reduction in pressure and temperature will have a significant effect on combustion. It is difficult to uncouple these effects from each other and, hence, determine whether the heat release makes any contribution to the wave propagation speed. The effect of heat release could be more effectively uncoupled from those of driver gas contamination by examining choking at the Mach 2.5 condition, for equivalence ratios of less than 0.4. At the lower Mach number condition, the choking occurs before the flow is contaminated.

## Conclusions

These experiments have shown that, when used together, shadowgraph visualization and static-pressure measurements may be used to determine when thermally induced choking of a model scramjet combustor occurs. The combination of techniques has been used to examine the propagation of the transient disturbance that characterizes the phenomenon at the two Mach number conditions examined. Previous experimental results have been confirmed by showing that the phenomenon may be avoided by using a divergent geometry in the combustor duct.

Some evidence that combustion has an effect on the propagation of the shock wave, in particular at the lower Mach number condition, has been provided by the shadowgraph images and the pressure measurements. The evidence is still insufficient to state categorically whether the effect of heat release is significant.

## Acknowledgments

The authors take the opportunity to acknowledge financial support from the Australian Research Council and the former Australian Space Office. The authors would like to gratefully acknowledge Paul Walsh and his associate Paul Tant for their operation of the T3 free-piston shock tunnel and construction of the diffuser. Thanks are also due to J. Shepherd, A. Paull, R. Boyce, and C. Morris for valuable advice on the behavior of detonation waves in supersonic premixed flowfields.

## References

[1]Curren, E. T., Heiser, W. H., and Pratt, D. T., "Fluid Phenomena in Scramjet Combustion Systems," *Annual Review of Fluid Mechanics*, Vol. 28, 1996, pp. 323–360.

[2]O'Byrne, S., Doolan, M., Olsen, S. R., and Houwing, A. F. P., "Measurement and Imaging of Supersonic Combustion in a Model Scramjet Engine," *Proceedings of the 21st International Symposium on Shock Waves*, Panther Publishing and Printing, Fyshwick, Australia, 1998, pp. 1119–1124.

[3]Stalker, R. J., "Development of a Hypervelocity Wind Tunnel," *Aeronautical Journal*, Vol. 76, June 1972, pp. 374–384.

[4]Stalker, R. J., and Morgan, R. G., "Supersonic Hydrogen Combustion with a Short Thrust Nozzle," *Combustion and Flame*, Vol. 57, 1984, pp. 55–70.

[5]McIntyre, T. J., Houwing, A. F. P., Palma, P. C., Rabbath, P. A. B., and Fox, J. S., "Optical and Pressure Measurements in Shock Tunnel Testing of a Model Scramjet Combustor," *Journal of Propulsion and Power*, Vol. 13, No. 3, 1997, pp. 388–394.

[6]Morgan, R. G., and Stalker, R. J., "Fast-Acting Hydrogen Valve," *Journal of Physics and Engineering: Scientific Instrumentation*, Vol. 16, March 1983, pp. 205–207.

[7]Casey, R., "An Investigation of Supersonic and Hypersonic Mixing and Combustion," Ph.D. Thesis, Dept. of Mechanical Engineering, University of Queensland, Brisbane, Australia, 1990.

[8]Yoon, Y., Donbar, J. M., Huh, H., and Driscoll, J. F., "Measured Supersonic Flame Properties: Heat Release Patterns, Pressure Losses, Thermal Choking Limits," *Journal of Propulsion and Power*, Vol. 12, No. 4, 1996, pp. 718–723.

[9]John, J. E. A., *Gas Dynamics*, Allyn and Bacon, Boston, 1984, pp. 218–224.

[10]Korkegi, R. H., "Comparison of Shock-Induced Two- and Three-Dimensional Incipient Turbulent Separation," *AIAA Journal*, Vol. 13, April 1975, pp. 534, 535.

[11]Waltrup, P. J., and Billig, F. S., "Prediction of Precombustion Wall Pressure Distributions in Scramjet Engines," *Journal of Spacecraft*, Vol. 10, No. 9, 1973, pp. 620–622.

[12]Rodi, P. E., Emami, S., and Trexler, C. A., "Unsteady Pressure Behavior in a Ramjet/Scramjet Inlet," *Journal of Propulsion and Power*, Vol. 12, No. 3, 1996, pp. 486–493.

[13]Ferri, A., "Review of Scramjet Propulsion Technology," *Journal of Aircraft*, Vol. 5, No. 1, 1968, pp. 3–10.